Random Walks, Fractons, and Electrons on Percolation Structures at Criticality

A. Bunde[1], J. Dräger[2,1] and J.W. Kantelhardt[1]

[1] Institut für Theoretische Physik, Justus-Liebig-Universität Giessen, Germany
[2] Institut für Theoretische Physik, Universität Hamburg, Germany

Abstract. We discuss the localization of random walks, vibrational excitations ("fractons"), and electronic wave functions on self similar percolation clusters at criticality. We show that, contrary to the common belief, the localization behavior of random walks differs basically from the behavior of fractons and electrons. This is seen best in the shortest path (chemical) metric: While the distribution of the probability densities at fixed chemical distance ℓ from the origin of the random walk is very narrow (for fixed time t), the distribution of the amplitudes of fractons and electrons at fixed ℓ from their localization is logarithmically broad (for eigenfunctions with fixed energy E or frequency ω). Here we present two different approaches that account for the different behavior of the considered localization phenomena. The treatments describe satisfactorily the numerical results, in particular the appearance of different localization regimes and the logarithmic dependence of the crossovers on the number of averaged configurations.

1 Introduction

It is well known that in disordered structures, random walks can be slowed down and electronic wave functions and vibrational excitations can be localized (Bunde et al. 1992, Kramer and MacKinnon 1993, Mookerjee et al. 1995, Nakayama et al. 1994), i. e., their amplitudes decrease with increasing distance from a localization center for certain energies E and frequencies ω, respectively. A standard model for disordered systems is the percolation model (Bunde and Havlin Eds. 1996, Stauffer and Aharony 1992). Close to the critical concentration, self-similar structures occur, and it is a challenging question, how the averaged eigenfunctions decay spatially on these structures and how this decay depends on the averaging procedure, especially on the number N of configurations taken into account in the average (Levy and Souillard 1987, de Vries et al. 1989; Roman et al. 1991, Lambert and Hughes 1991, Bunde and Roman 1992, Aharony and Harris 1992, Bunde and Dräger 1995, Dräger et al. 1995, Kantelhardt and Bunde 1997). Closely related to this problem is, how the probability density of a random walker decreases with increasing distance r from the starting point of the random walk (Bunde and Havlin Eds. 1996, Havlin and Ben-Avraham 1987, Bouchaud and Georges 1990, Kehr and Kutner 1982; Havlin et al. 1985, O'Shaughnessy and Procaccia 1985, Bunde et al. 1990, Eisenberg et al. 1994). Apart from its

principal relevance, the knowledge of the localization behavior in disordered self-similar systems is relevant for a large number of both experimental and theoretical issues, ranging from neutron and light scattering (Tsujimi et al. 1988, Montagna et al. 1990, Stoll et al. 1992) to the thermally activated hopping conductivity in disordered systems (Deutscher et al. 1987; Harris and Aharony 1987, van der Putten et al. 1992; 1993; Aharony et al. 1993, Mandal et al. 1997).

In this article, we review our previous work on the localization of random walks, fractons and electrons on percolation clusters at criticality. According to this purpose, the paper is organized as follows. First, in Section 2, we give an introduction to standard percolation theory. In Section 3, we discuss random walks, while Sections 4 and 5 deal with vibrational excitations ("fractons") and electronic wave functions on percolation clusters.

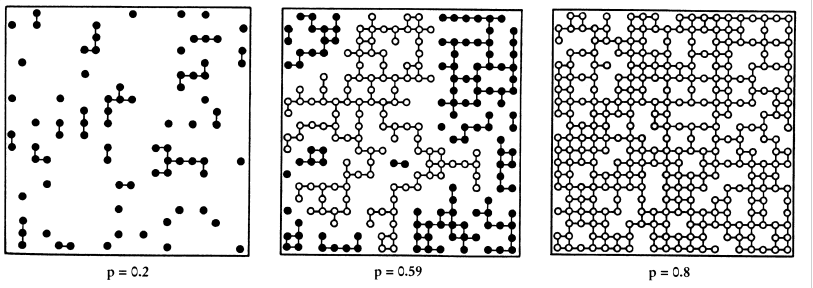

Fig. 1. Site percolation on the square lattice: The small circles represent the occupied sites for three different concentrations: $p = 0.2$, 0.59, and 0.80. Nearest-neighbor cluster sites are connected by lines representing the bonds. Filled circles are used for finite clusters, while open circles mark the large *infinite* cluster.

2 Percolation Theory: A Brief Introduction

Percolation represents a standard model for a structurally disordered system (for recent reviews with applications see (Bunde and Havlin Eds. 1996, Stauffer and Aharony 1992, Sahimi 1994)). Let us consider a square lattice, where each site is chosen to be occupied randomly with probability p or empty with probability $1 - p$ (see Fig. 1). Occupied and empty sites may stand for very different physical properties. For illustration, let us assume that the occupied sites are electrical conductors, while the empty sites represent insulators, and that electrical current can flow only between nearest-neighbor conductor sites.

At low concentration p, the conductor sites are either isolated from each other or form small clusters. Two conductor sites belong to the same cluster if they are connected by a path of nearest-neighbor conductor sites. At low values of p, the mixture is an insulator, since no conducting path connecting opposite edges of the lattice exists. At large values of p, on the other hand, many conducting paths between opposite edges exist, where electrical current can flow, and the mixture is a conductor. At some concentration in between, therefore, a threshold concentration p_c must exist where for the first time electrical current can *percolate* from one edge to the other. Below p_c we have an insulator, above p_c we have a conductor. The threshold concentration is called the *percolation threshold,* or, since it separates two different phases, the *critical concentration.*

If the occupied sites are superconductors and the empty sites are conductors, p_c separates a normal-conducting phase below p_c from a superconducting phase above p_c. Another example is a mixture of ferromagnets and paramagnets, where the system changes at p_c from paramagnetic to ferromagnetic.

In contrast to the more common thermal phase transitions, where the transition between two phases occurs at a critical temperature, the *percolation transition* described here is a *geometrical phase transition,* which is characterized by the geometric features of large clusters in the neighborhood of p_c. At low values of p only small clusters of occupied sites exist. When the concentration p is increased the average size of the clusters increases. At the critical concentration p_c a large cluster appears which connects opposite edges of the lattice. We call this cluster the *infinite* cluster, since its size diverges in the thermodynamic limit. When p is increased further the density of the infinite cluster increases, since more and more sites belong to the infinite cluster while the average size of the *finite* clusters decreases.

The percolation threshold depends on the details of the lattice and increases, for fixed dimension d of the lattice, with decreasing coordination number z of the lattice: For the triangular lattice, $z = 6$ and $p_c = 1/2$, for the square lattice, $z = 4$ and $p_c \cong 0.592746$, and for the honeycomb lattice, $z = 3$ and $p_c \cong 0.6962$. For fixed z, p_c decreases if the dimension d is enhanced: For the triangular lattice as well as for the simple cubic lattice we have $z = 6$, but p_c for the simple cubic lattice is considerably smaller, $p_c \cong 0.3116$.

The percolation transition is characterized by the geometrical properties near p_c (Bunde and Havlin Eds. 1996, Stauffer and Aharony 1992). The probability P_∞ that a site belongs to the infinite cluster is zero below p_c and increases above p_c as

$$P_\infty \sim (p - p_c)^\beta, \tag{1}$$

with $\beta = 5/36$ in $d = 2$ and $\beta \approx 0.417$ in $d = 3$. The linear size of the *finite* clusters, below and above p_c, is characterized by the *correlation length* ξ. The correlation length is defined as the mean distance between two sites

on the same finite cluster and represents the characteristic length scale in the system. When p approaches p_c, ξ increases as

$$\xi \sim \mid p - p_c \mid^{-\nu}, \tag{2}$$

with the same exponent ν below and above the threshold ($\nu = 4/3$ in $d = 2$ and $\nu \approx 0.875$ in $d = 3$). While p_c depends explicitly on the type of the lattice, the *critical exponents* β and ν are universal, i.e. they depend only on the dimension d of the lattice.

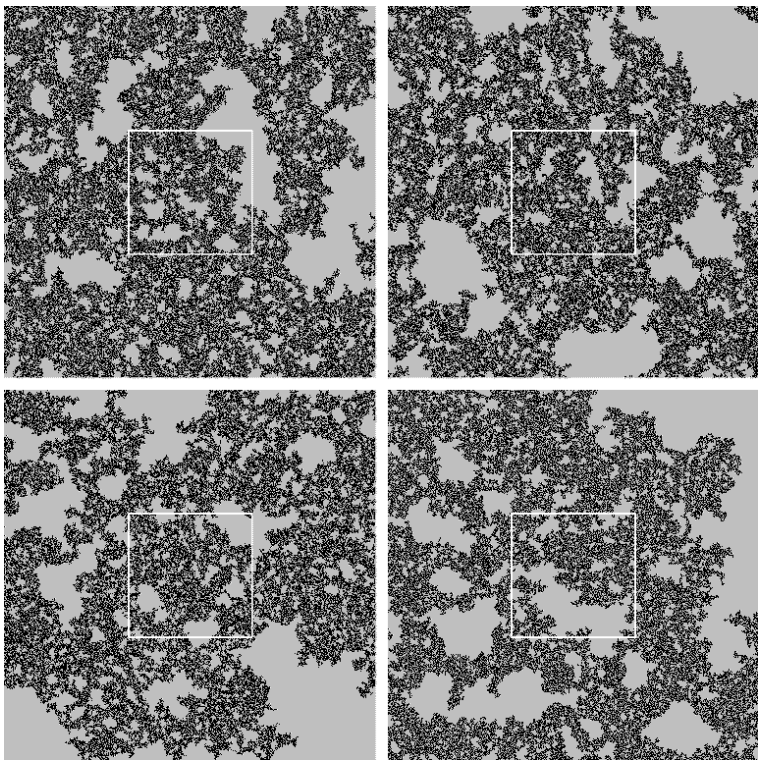

Fig. 2. Self-similarity of a large percolation cluster on the square lattice at the critical concentration. Three of the clusters are magnifications of the center parts marked by white squares.

Near p_c on length scales smaller than ξ both the infinite cluster and the finite clusters are self-similar, i.e., if we cut a small part out of a large cluster, magnify it to the original cluster size and compare it with the original, we

cannot tell the difference: Both look the same. This feature is illustrated in Fig. 2, where a large cluster at p_c is shown in four different magnifications. We leave it to the reader to find out what is the original and what are the magnifications.

As a consequence of the self-similarity the cluster is characterized by a "fractal" dimension d_f, which is smaller than the dimension d of the embedding lattice. The mean mass of the cluster within a circle of radius r increases with r as $M(r) \sim r^{d_f}$ with $d_f = 91/48$ in $d = 2$ and $d_f \approx 2.524$ in $d = 3$. Above p_c on length scales *larger* than ξ the infinite cluster can be regarded as an homogeneous system which is composed of many cells of size ξ. Mathematically, this can be summarized as

$$M(r) \sim \begin{cases} r^{d_f}, & \text{if } r \ll \xi \\ r^{d}, & \text{if } r \gg \xi \end{cases} . \tag{3}$$

The fractal dimension d_f is related to β and ν by $d_f = d - \beta/\nu$. Since β and ν are universal exponents, d_f is also universal.

The fractal dimension d_f is not sufficient to fully characterize the infinite percolation cluster, since the cluster contains several fractal substructures. The most important fractal substructure for transport phenomena is the shortest path connecting two sites on the cluster. The length ℓ of the shortest path is called the "topological" (or "chemical") distance. The mean chemical distance ℓ between two sites at spatial distance r from each other scales as

$$\ell(r) \sim r^{d_{\min}} , \tag{4}$$

with the fractal dimension of the minimum path $d_{\min} \approx 1.13$ in $d = 2$ and $d_{\min} \approx 1.374$ in $d = 3$. Another exponent, the "topological" (or "chemical") dimension d_ℓ describes how the mean cluster mass M scales with the chemical distance ℓ,

$$M(\ell) \sim \ell^{d_\ell} . \tag{5}$$

By combining equations (3), (4) and (5) one obtains $d_\ell = d_f/d_{\min}$ yielding $d_\ell \approx 1.678$ (1.84) for percolation in $d = 2$ (3).

Equations (3)-(5) represent the first moments of the corresponding distribution functions. For a more microscopic description we need to calculate the distribution of the chemical distances between two sites at fixed spatial distance r. We denote by $\phi(\ell|r)d\ell$ the probability of finding a value within $d\ell$ of ℓ. Numerically $\phi(\ell|r)$ is extracted by averaging the ratio $S(\ell, r)/S(r)$ over N configurations, where $S(r)$ is the number of sites at distance r and $S(\ell, r)$ is the number of sites among these $S(r)$ sites that are at chemical distance ℓ.

Due to selfsimilarity $\phi(\ell|r)$ is a scaling function of the variable $x = r/\ell^{1/d_{\min}}$. In analogy to random walk trails, $\phi(\ell|r)$ is expected to have the functional form

$$\phi(\ell|r) \sim \frac{1}{\ell} x^g \exp\left[-A \cdot x^\delta\right] , \tag{6}$$

with $\delta = d_{\min}/(d_{\min}-1)$. The factor $1/\ell$ follows from the normalization $\int \phi(\ell|r)d\ell = 1$. Numerical simulations yield $g \cong 1.14$ (1.34) for percolation in $d = 2$ (3). According to (6), $\phi(\ell|r)$ increases exponentially with ℓ until the maximum at $\ell_{\max}(r) \simeq r^{d_{\min}}$ is reached. For larger ℓ values, $\phi(\ell|r)$ decreases by a power law. $\phi(\ell|r)$ is zero below a cutoff distance $\ell_{\min}(r,N)$ that depends on the number of configurations N taken into account in the average. For ℓ below a crossover distance $r_{\rm c}(N)$, one has simply $\ell_{\min}(r,N) = r$ (because the topological distance ℓ cannot be shorter than the spatial distance r), while above $r_{\rm c}(N)$,

$$\ell_{\min}(r,N) \sim r_c(N)^{1-d_{\min}} r^{d_{\min}}, \quad r > r_c(N)\,. \tag{7}$$

The crossover distance $r_c(N)$ is given by (Bunde and Dräger 1995)

$$r_c(N) = (\ln z + \ln N)/\ln(1/p_c)\,, \tag{8}$$

where z is the coordination number of the lattice.

As we will see below the structural function $\phi(\ell|r)$ and its cutoff value $\ell_{\min}(r,N)$ play a crucial role for calculating the averaged probability density of random walks on percolation clusters.

3 Diffusion

We first consider a random walker on a lattice of dimension d. The random walker can hop between accessible nearest neighbor sites. The probability for the random walker to be at site n of the lattice satisfies the discretised diffusion equation,

$$\frac{dP_n(t)}{dt} = \sum_m {\rm w}_{n,m}[P_m(t) - P_n(t)]\,. \tag{9}$$

The sum runs over all nearest neighbor sites m of site n. Since the random walker starts at time $t = 0$ at site k, the initial condition is $P_n(t=0) = \delta_{nk}$. On a regular lattice, the hopping probabilities ${\rm w}_{n,m}$ are given by ${\rm w}_{n,m} = 1/z$, where z is the coordination number. The probability density for the random walker on a site depends only on the distance r from the origin of the walk and is (for $t \gg r$) given by

$$P(r,t) = P(0,t)\exp\left[-\frac{d\,r^2}{R(t)}\right]\,, \tag{10}$$

where

$$R^2(t) \equiv \langle r^2(t)\rangle = 2dt\,, \tag{11}$$

and $P(0,t) = (2\pi t)^{-d/2}$.

Next we consider a random walker on the infinite percolation cluster at the critical concentration p_c. The random walker can hop between occupied

nearest neighbor sites. The probability $P_n(t)$ to find the random walker at time t at site n of the considered configuration obeys the rate equation (9). The hopping probabilities are $w_{n,m} = 1/z$ if both sites belong to the same cluster and 0 otherwise.

In order to describe the spatial decay of the probability density of the random walker after t time steps one has to average over all probabilities $P_n(r,t)$ at sites n at fixed distance r from the starting point of the walk. In contrary to the case of a regular structure described above, these probabilities may have very different values. To calculate the average value of the probability density, two averages must be employed. First we average $P_n(r,t)$ for a given configuration over all sites n at spatial distance r from the origin of the walk, and obtain

$$P_\nu(r,t) \equiv \frac{1}{S_\nu(r)} \sum_{n=1}^{S_\nu(r)} P_n(r,t)\,, \tag{12}$$

where $S_\nu(r)$ is the number of sites at distance r from the origin of the walk of the νth configuration. Then we average $P_\nu(r,t)$ over N configurations,

$$\langle P(r,t)\rangle_N \equiv \frac{1}{N} \sum_{\nu=1}^{N} P_\nu(r,t)\,. \tag{13}$$

First we consider $R(t)$ on the infinite percolation cluster. Due to the loops and dangling ends on the cluster, the motion of the random walker is slowed down. Since these loops and dangling ends occur on all length scales, the motion of the random walker is slowed down on all length respectively time scales. The time t the walker needs to travel a distance r is no longer proportional to r^2, but scales as $t \sim r^{d_w}$, where $d_w > 2$ is the *anomalous diffusion exponent* (Bunde and Havlin Eds. 1996, Stauffer and Aharony 1992). Accordingly the root-mean-square displacement $R(t)$ scales as

$$R(t) \sim t^{1/d_w}\,. \tag{14}$$

The exponent d_w is approximately equal to $3d_f/2$ (Alexander and Orbach 1982). Numerical simulations yields $d_w \approx 2.87$ for percolation in $d = 2$ and $d_w \approx 3.80$ for percolation in $d = 3$.

From $R(t)$ one can easily derive the scaling behavior of the probability $\langle P(0,t)\rangle$ that, after t time steps, the random walker is at the origin of the walk. Since the averaged spatial volume V explored by the random walker at time t scales as $V \sim R(t)^{d_f}$, $\langle P(0,t)\rangle$ scales as

$$\langle P(0,t)\rangle \sim 1/V \sim 1/R(t)^{\,d_f} \sim t^{-d_f/d_w}\,. \tag{15}$$

While the averaged probability density $\langle P(r,t)\rangle_N$ shows a very complicated behavior, as it will be pointed out below, the situation becomes very different if the probability density at fixed chemical distance ℓ is regarded. As mentioned already in Section 2 the chemical distance ℓ is the length of

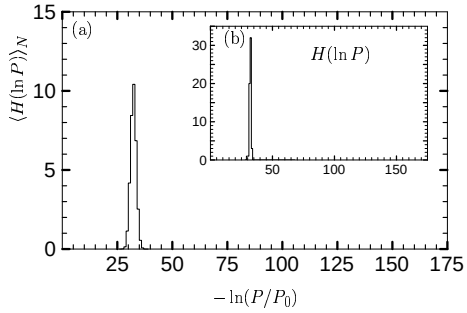

Fig. 3. Plot of the histogram $H(\ln P)$ versus $\ln(P/P_0)$ for percolation clusters in $d = 2$ for fixed $\ell = 100$ and $t = 2000$ (a) averaged over 10^3 configurations and (b) for a single configuration.

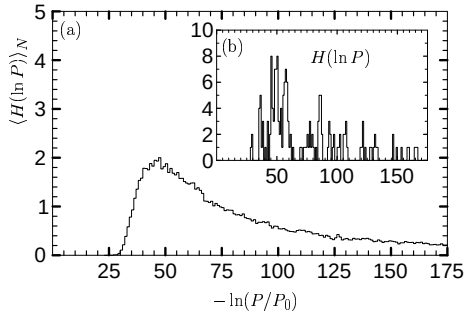

Fig. 4. Plot of the histogram $H(\ln P)$ versus $\ln(P/P_0)$ for percolation clusters in $d = 2$ for fixed $r = 70$ and $t = 2000$ (a) averaged over 10^3 configurations and (b) for a single configuration.

the shortest path connecting two points on the structure. Figure 3 shows the histogram $H(\ln(P))$ defined as the number of sites with probability density $\ln(P)$ between $\ln(P)$ and $\ln(P) + d\ln(P)$ (for fixed ℓ and t), (a) for a large number N of configurations and (b) for a single configuration. The corresponding histograms for fixed r are represented in Fig. 4. The comparison of Figs. 3 and 4 clearly shows that the fluctuations at fixed chemical distance ℓ from the origin are considerably smaller than the fluctuations at fixed Euclidean distance r. Therefore the chemical distance ℓ and *not* the Euclidean distance r is the relevant physical length scale for the diffusion problem on percolation. This leads to the reasonable assumption that approximately all sites n at fixed chemical distance ℓ from the origin have the same probability density $\langle P(\ell, t)\rangle$. As predicted by scaling theory, $\langle P(\ell, t)\rangle$ scales as

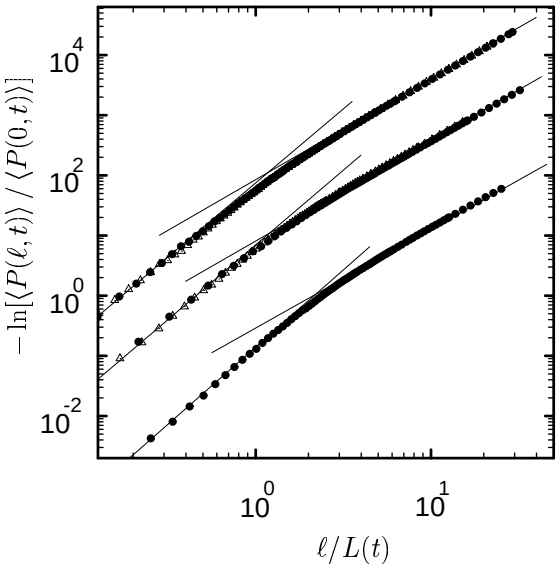

Fig. 5. Random walks on random fractals in the *chemical* space: Scaling plot of $-\ln(\langle P(\ell,t)\rangle / \langle P(0,t)\rangle)$ as a function of $\ell/L(t)$ for (a) percolation clusters in $d=2$ for $t=5000$ (circles) and $t=10000$ (triangles), (b) percolation clusters in $d=3$ for $t=1000$ (circles) and $t=5000$ (triangles), (c) for the Cayley-tree for $t=2000$ (circles) and $t=5000$ (triangles). The two lines in the plots represent the theoretical slopes with effective exponents $d_{\rm w}$ taken at the time instances.

$\langle P(\ell,t)\rangle / \langle P(0,t)\rangle = f(\ell/L(t))$ where $L(t)$ is the mean chemical distance the random walker has travelled at time t. Figure 5 shows that at large ℓ the probability density in ℓ-space $\langle P(\ell,t)\rangle$ is given by

$$-\ln\langle P(\ell,t)\rangle \sim \left(\frac{\ell}{L(t)}\right)^{v}, \quad \ell \gg L(t)\,, \tag{16}$$

with $v = d_{\rm w}/(d_{\rm w}-d_{\rm min})$ (see also (Havlin and Ben-Avraham 1987)). At small values of ℓ the slopes are consistent with $\tilde{v} = d_{\rm w}/d_{\rm min}$ (Dräger and Bunde 1996),

$$-\ln\langle P(\ell,t)\rangle \sim \left(\frac{\ell}{L(t)}\right)^{\tilde{v}}, \quad \ell \ll L(t)\,. \tag{17}$$

A similar crossover behavior has been observed earlier for random walks on the Sierpinski-gasket where ℓ scales linearly with r (Kafter et al. 1991).

Since the fluctuation of the probability densities at fixed chemical distance ℓ from the origin of the random walk are negligible, for both the same and different configurations, $\langle P(r,t)\rangle$ can be written as a convolutional integral

between $\langle P(\ell,t)\rangle$ and the probability $\phi(\ell|r)$ (see (6)) that two sites with Euclidean distance r are at chemical distance ℓ from each other ((Bunde and Dräger 1995), see also (Bunde et al. 1990)),

$$\langle P(r,t)\rangle_N = \int_{\ell_{\min}(r,N)}^{\infty} \phi(\ell|r)\,\langle P(\ell,t)\rangle\; d\ell\,. \tag{18}$$

Equation (18) reveals that averaging $\langle P(r,t)\rangle_N$ involves both a simple arithmetic average ($\phi(\ell|r)$) that is independent of N for large N and a minimization procedure leading to the structural quantity $\ell_{\min}(r,N)$ (see Section 2). The integral (18) can be calculated analytically by using (6) and (16). In the asymptotic regime $r > R(t)$ where only large ℓ-values contribute to the convolution integral (i.e. $\langle P(\ell,t)\rangle$ is given by (16)) the method of steepest descent yields ((Bunde and Dräger 1995), see also (Bunde et al. 1990))

$$-\ln\langle P(r,t)\rangle_N \sim \left(\frac{r}{R(t)}\right)^u\,, \tag{19}$$

with $u = d_w/(d_w-1)$. Since the saddle point $\ell^* \sim R(t)^{d_{\min}}[r/R(t)]^{u/v}$ has to be within the integration regime (i. e. $\ell_{\min}(r,N) < \ell^*$), (19) can be only valid for r below the crossover length

$$r_\times(N) \sim R(t)\, r_c^{1/u}(N)\,, \tag{20}$$

with $r_c(N)$ from (8). For $r > r_\times(N)$ the integrand in (18) is peaked sharply at $\ell = \ell_{\min}(r,N)$, and

$$-\ln\langle P(r,t)\rangle_N \sim r_c(N)^{v(1-d_{\min})}\left(\frac{r}{R(t)}\right)^{v\,d_{\min}}\,, \qquad r > r_\times(N)\,. \tag{21}$$

We like to note that for r below $R(t)$, the saddle point ℓ^* is smaller than the maximum $\ell_{\max}(r)$ of the structural function $\phi(\ell|r)$. In this case the evaluation of (18) leads to a non-exponential localization behavior in r-space (Dräger et al. 1995).

Above $R(t)$, the results (19)-(21) for the asymptotic regime $r > R(t)$ can be summarized by

$$-\ln\langle P(r,t)\rangle_N = r_\times(N)^u\left(\frac{r}{r_\times(N)}\right)\,, \tag{22}$$

with $f(x) \sim x^u$ for $x \ll 1$ and $f(x) \sim x^{d_{\min}v}$ for $x \gg 1$.

Equations (19)-(22) show that at large distances r the relevant length scale increases *logarithmically* with the number N of configurations, and conventional scaling and self-averaging breaks down. Below $r_\times(N)$ (see (20)), $\langle P(r,t)\rangle$ is independent of N and described by the exponent $u = d_w/(d_w-1)$. Above $r_\times(N)$, $\langle P(r,t)\rangle_N$ depends logarithmically on N and is described by

the exponent $vd_{\min} = d_{\min} d_w/(d_w - d_{\min})$. The origin of this non selfaveraging behavior is the anomalous broadness of the distribution of the probability densities for fixed r and t. This also leads to multifractal behavior of the corresponding moments (Dräger and Bunde 1996). Due to the multifractality, the first moment $\langle P(r,t)\rangle$ of the distribution scales different than the maximum. For very large r-values, $\langle P(r,t)\rangle$ is mainly determined by the cutoff value of the distribution that naturally depends on the number of configurations contributing to the distribution. While for the diffusion on percolation clusters the cutoff of the distribution is determined by the structural quantity $\ell_{\min}(r, N)$, a different approach is necessary for the distribution of amplitudes of localized electronic wave functions and fractons. Nevertheless the logarithmical broadness of the distribution is the deeper reason for the N-dependence of the first moment for the considered anomalous localization phenomena.

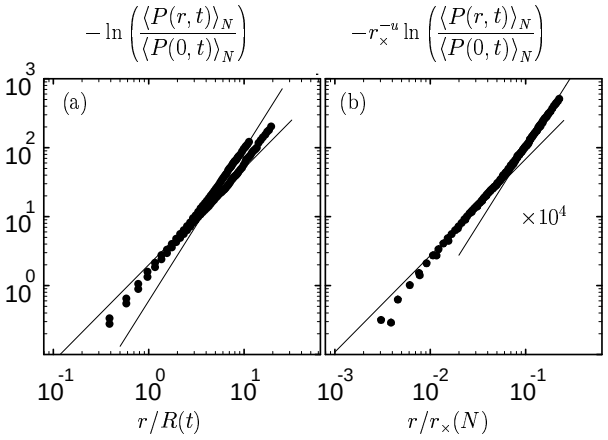

Fig. 6. (a) Logarithm of the mean probability density $-\ln(\langle P(r,t)\rangle_N/\langle P(0,t)\rangle_N)$ of random walks versus $r/\langle R(t)\rangle$ for site percolation clusters on the simple cubic lattice ($t = 1000$, $N = 1$ (full circles) and 125 (stars); $\langle R(t)\rangle$ is the root-mean-square displacement. (b) Scale plot $-\ln(\langle P(r,t)\rangle_N/\langle P(0,t)\rangle_N)/r_\times^u(N)$ versus $r/r_\times(N)$ for site percolation clusters on the simple cubic lattice, both for the same N values as in (a).

Figure 6 represents the numerical results of Monte-Carlo simulations of random walks on site percolation clusters on the simple cubic lattice (Bunde and Dräger 1995). Figure 6(a) shows the typical average of $\langle P(r,t)\rangle_N$ for $N = 1$ and 200 configurations. The typical average has been obtained in the way described above, but to smoothen the results, it has been averaged logarithmically over many sets of N configurations. The N-dependent crossover

is clearly seen. The slopes of the curves correspond to the theoretical predictions for percolation in $d = 3$. Figure 6(b) shows the validity of the scaling relation for both averages with different values of N.

Our analytic calculations become exact for linear fractal structures like random walk trails and self avoiding random walks (Bunde and Dräger 1995), where the probability density in ℓ-space is simply given by a Gaussian ($v = 2$). For linear fractal structures the formalism can be applied (with $v = 1$ in (16)) also to localized vibrations and (pinned) electrons (Bunde and Dräger 1995) where the localization is caused by additional disorder (smaller mass or deeper potential well in the origin of the chain). In these cases, the distribution of the amplitudes at fixed ℓ values can be approximated by a δ-function. In the case we consider next, localization is generated by more complicated structural interferences. As we shall see, the fluctuations of the amplitudes in ℓ-space cannot be neglected, since the amplitudes for fixed ℓ are anomalously broadly distributed.

4 Fractons

We consider site percolation clusters at the critical concentration p_c and assume that equal masses M are placed on each occupied site. Nearest neighbor cluster sites are coupled by (scalar) force constants $k_{n,m}^{\alpha,\beta} = k_{n,m}^{\beta,\alpha} = k_{n,m}$, where n, m are the site indices and α, β are the directional indices. In this case, different components of displacements decouple and we obtain the same vibrational equation for all components $u_n(t)$,

$$M \frac{d^2}{dt^2} u_n(t) = \sum_m{}' k_{n,m} \ [u_m(t) - u_n(t)] \ , \tag{23}$$

where the sum runs over all nearest neighbor sites m of site n. The ansatz $u_n(t) = u_n(\omega) \cdot \exp(-i\omega t)$ leads to the time independent vibration equation (Alexander and Orbach 1982, Nakayama et al. 1994, Bunde and Havlin Eds. 1996),

$$\left(-\omega^2 + N_n\right) \ u_n(\omega) = \sum_m{}' u_m(\omega) \, . \tag{24}$$

Here, N_n is the number of occupied nearest neighbor sites m of site n. The force constants $k_{n,m}$ are equal to k for nearest neighbor cluster sites and zero otherwise; for simplicity we set $k/M = 1$ which determines the frequency unit. Equation (23) is an eigenvalue equation for eigenfrequencies ω and the corresponding eigenvectors $u_n(\omega)$. Since the vibrational equation (23) is identical to the diffusion equation (9) if we replace the second derivative by the first one, the eigenfunctions are identical for the diffusion problem and the vibrational problem. Thus, the localization behavior had been expected to be similar for both problems (Bunde et al. 1992, Bunde and Havlin Eds. 1996, Stauffer and Aharony 1992, Bunde and Dräger 1995). But, as we shall

see, the similarity between the two equations does only determine the scaling of the density of states and of the wavelength of the fractons, while their localization behavior turns out to be different from the diffusion problem.

On regular lattices without disorder, the eigenstates of (24) are extended sound waves (phonons). Their density of states scales as $g(\omega) \sim \omega^{d-1}$, where d is the space dimension, and their wavelength λ is determined by the common dispersion relation $\lambda = 2\pi c/\omega$. On fractal structures like the infinite percolation cluster at p_c, the eigenstates become localized, and were termed "fractons" by Alexander and Orbach (Alexander and Orbach 1982). For the fracton density of states, the space dimension d is replaced by the spectral dimension $d_s = 2d_f/d_w \approx 4/3$: $g(\omega) \sim \omega^{d_s-1}$. The analogy to diffusion can be employed, to some extent, to determine the characteristic wavelength λ of the fractons, which scales as $\lambda \sim \omega^{-2/d_w}$.

The quantities corresponding to the probability densities $P(\ell, t)$ and $P(r, t)$ are the fracton amplitudes $u(\ell, \omega)$ and $u(r, \omega)$ determined similarly to (12) by averaging over all amplitudes $|u_n(\omega)|$ at fixed distances ℓ respectively r from the localization center. Here, the localization center is defined for each individual eigenfunction as the site n, where $|u_n(\omega)|$ takes its maximum. The averaging procedure for different configurations is the same as for the diffusion probabilities (see (13)). It determines the N dependent averages $\langle u(\ell, \omega)\rangle_N$ and $\langle u(r, \omega)\rangle_N$. For nomalization, we divide the amplitudes by their maximum value $|u(0)|$.

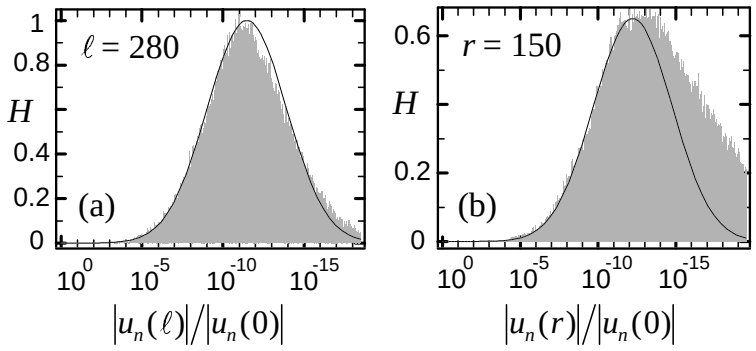

Fig. 7. (a) Histogram of the amplitudes $|u_n(\ell)/u(0)|$ for fractons on critical percolation clusters in $d = 2$ at fixed chemical lengths $\ell = 280$ from the localization center. (b) Histogram of the amplitude values $|u_n(\ell)/u(0)|$ for fixed Euclidian lengths $r = 150$. The continuous lines represent Gaussian fits to the data according to (25) and the corresponding function for r-space with the parameters $\lambda_\ell = 10.6$, $\sigma = 2.4$, $\lambda_r = 5.4$, and $A = 0.65$.

While the distribution of the probability densities $P_n(\ell, t)$ is very narrow for fixed ℓ and t, a logarithmically broad distribution is found for fractons already in ℓ-space. Figure 7(a) shows the histogram of the amplitudes $|u_n(\ell)/u(0)|$ for a fixed distance ℓ from the center of localization. To obtain the histogram, the amplitudes of 10^3 eigenfunctions of (24) for similar frequencies ω were calculated numerically using the Lanczos algorithm. The figure shows that the histogram obeys a log-normal distribution (Kantelhardt and Bunde 1997),

$$H(x, \ell) = \frac{1}{\sqrt{\pi\sigma\ \ell/\lambda_\ell}}\ \exp\left[-\frac{(x - \ell/\lambda_\ell)^2}{\sigma\ \ell/\lambda_\ell}\right], \tag{25}$$

where $x = |\ln|u_n(\ell)/u(0)|| \geq 0$. The continuous line in Fig. 7(a) corresponds to (25) with $\lambda_\ell = 10.6$ and $\sigma = 2.4$, and fits the numerical data surprisingly well, especially for large ℓ. Note that the parameter λ_ℓ is the localization length, since the amplitude $|u_n(\ell)| = |u(0)|\exp(-\ell/\lambda_\ell)$ occurs with the largest probability at the topological distance ℓ from the center of localization according to (25). Although the distribution of the amplitudes turns out to be very different from the random walk case, it still has a surprisingly simple form in ℓ space. Only for small chemical distances $\ell < \lambda_\ell$ from the localization center, deviations from the log-normal form occur.

For fixed distance r from the center of localization the distribution of the amplitudes is not exactly log-normal, as can be seen in Fig. 7(b); the figure corresponds to Fig. 7(a) for the ℓ-space. But the distribution of the relevant large amplitudes $|u_n(r)|$ can surprisingly well be approximated by a log-normal fit. The continuous line in Fig. 7(b) represents a fit to the left part of the histogram by the (renormalized) log-normal distribution $H(x, r) = A/(\pi\sigma r/\lambda_r)^{1/2}\ \exp[-(x - r/\lambda_r)^2/(\sigma r/\lambda_r)]$ (similar to $H(x, \ell)$ in (25)) with the parameters $\lambda_r = 5.4$, $\sigma = 2.4$, and $A = 0.65$ and $x = |\ln|u_n(r)/u(0)||$. The right part corresponds to very small values of $u_n(r)$, and therefore is not essential for the calculation of arithmetical averages.

Since we can approximate very well the distribution of dominating amplitudes $|u_n(\ell)|$ at chemical distances $\ell \gg \lambda_\ell$ by (25), we can calculate the average $\langle u(\ell)\rangle_N$ for large ℓ by simple integration. In particular, we can obtain $\langle u(\ell)\rangle_N$ in the asymptotic regime which is not accessible numerically. We can also estimate the way $\langle u(\ell)\rangle_N$ depends on the number of averaged configurations N.

If we average over all configurations, the resulting quantity $\langle u(\ell)\rangle_\infty$ is related to $H(x, \ell)$ by

$$\langle u(\ell)\rangle_\infty = \int_0^\infty e^{-x}\ H(x, \ell)\, dx\,. \tag{26}$$

Straightforward integration yields

$$\langle u(\ell)\rangle_\infty = \exp\left[\frac{(\sigma/4-1)\ell}{\lambda_\ell}\right] \frac{1-\mathrm{erf}\left[(\sigma/2-1)\sqrt{\ell/\lambda_\ell\sigma}\right]}{1+\mathrm{erf}\left[\sqrt{\ell/\lambda_\ell\sigma}\right]}\,. \tag{27}$$

For a *finite* number N of configurations, the total number of sites at distance ℓ from the localization center is identical to $N\langle N_\ell\rangle$ with $\langle N_\ell\rangle = a\ \ell^{d_\ell-1}$ (a = const). Clearly, those values of $x = |\ln|u_n(\ell)/u(0)||$ with a too small probability $[H(x,\ell) < 1/(N\langle N_\ell\rangle)]$ are unlikely to occur in N typical configurations, and the condition $H(x_{\min},\ell) = 1/(N\langle N_\ell\rangle)$ determines a lower cutoff value

$$x_{\min}(\ell,N) = \max\left[0, \frac{\ell}{\lambda_\ell} - \sqrt{\frac{\sigma\ell}{\lambda_\ell}\ \ln\left(aN\ell^{d_\ell-3/2}\sqrt{\lambda_\ell/\pi\sigma}\right)}\right]\,, \tag{28}$$

which replaces the lower integration bound in (26) for finite N,

$$\langle u(\ell)\rangle_N = \int_{x_{\min}(\ell,N)}^{\infty} e^{-x}\ H(x,\ell)\,dx\,. \tag{29}$$

The integration can be performed straightforwardly and gives

$$\langle u(\ell)\rangle_N \cong \frac{1}{2}\ \exp\left[\frac{(\sigma/4-1)\ell}{\lambda_\ell}\right]\cdot$$
$$\cdot\left\{1-\mathrm{erf}\left[\sqrt{\frac{\sigma\ell}{4\lambda_\ell}} - \sqrt{\ln\left(aN\ell^{d_\ell-3/2}\sqrt{\lambda_\ell/(\pi\sigma)}\right)}\right]\right\}\,. \tag{30}$$

This result is supposed to be rigorous for sufficiently large ℓ-values ($\ell \gg \lambda_\ell$), where the distribution of $|u_n(\ell)|$ is described by the log-normal distribution $H(x,\ell)$. It can be shown that (30) is equivalent to an ℓ dependent effective localization exponent $\nu > 1$ in (16) approaching $\nu = 1$ in the limit $\ell \to \infty$. Equation (30) is not valid for small ℓ-values, for which the lower integration limit $x_{\min}(\ell,N)$ in (29) tends to zero. For sufficiently small ℓ-values, the real distribution of $|u_n(\ell)|$ deviates from the log-normal distribution $H(x,\ell)$ for small x-values corresponding to large $|u_n(\ell)|$. In this case, the log-normal approximation is inappropriate, and therefore cannot yield exact results for $\langle u(\ell)\rangle_N$.

Despite of this, the log-normal approximation can be used for obtaining a qualitative picture of $\langle u(\ell)\rangle_N$ even at small ℓ-values, where $x_{\min}(\ell,N) = 0$. In this case we come back to (26) and find $\langle u(\ell)\rangle_N \approx \langle u(\ell)\rangle_\infty$ (see (27)) for the intermediate localization regime $\lambda_\ell < \ell < \ell_\times(N)$. It can be shown, that (27) yields an effective localization exponent $\nu \approx 0.6$ in ℓ-space ("sublocalization", see (16)).

Furthermore, we can obtain a qualitative description of the logarithmic N-dependence of the crossover length $\ell_\times(N)$ separating the two localization regimes, if we identify $\ell_\times(N)$ with the largest distance ℓ for which the condition $x_{\min}(\ell,N) = 0$ holds. This yields (with (28))

$$\ell_\times(N) = \lambda_\ell \, \sigma \, [2 \ln N + (2d_\ell - 3) \ln \ell_\times(N) - \ln(a^2 \pi \sigma / \lambda_\ell)]/2 \,, \qquad (31)$$

which is an implicit equation for $\ell_\times(N)$. As described above, we cannot expect to find a quantitative agreement here, since the log-normal distribution function $H(x, \ell)$ does not fit well for very small x values. For $N \gg 1$ (31) reduces to $\ell_\times(N) \approx \lambda_\ell \sigma \ln N$. The logarithmic dependence of $\ell_\times(N)$ on N reminds of the logarithmic dependence of $r_\times(N)$ in the diffusion problem.

It is remarkable that by this analytic approach, the essential complex features of the localization phenomenon, sublocalization in the intermediate regime, crossover to superlocalized behavior (that depends on the number of configurations N), and final approach to simple exponential behavior asymptotically, are reproduced. Our theoretical description is also appropriate for describing the localization behavior as a function of the spatial distance r, even though the distribution of $|u_n(r)|$ for fixed r has a more complicated shape than in ℓ-space. But since the log-normal distribution fits the left part of the distribution of $|u_n(r)|$ quite well, the calculations in this section can simply be transferred to r-space by replacing ℓ by r, λ_ℓ by λ_r, and d_ℓ by the fractal dimension d_f in (26) to (31). Accordingly, since the widths σ of the distributions turn out to be the same, we obtain the same localization behavior for $\langle u(\ell) \rangle_N$ and $\langle u(r) \rangle_N$.

The numerical results shown in Figs. 8 and 9 confirm this theoretical description. In Fig. 8 the averaged fracton amplitudes on percolation clusters of the Cayley tree with $z = 3$ at the critical concentration $p_c = 0.5$ are shown versus the topological distance ℓ. The two localization regimes corresponding to (27) and (30) can clearly be seen. In the intermediate regime, for $\lambda_\ell < \ell \ll \ell_\times(N)$, (27) holds approximately. There we find averaged amplitudes $\langle u(\ell) \rangle_N$ decaying slower than a simple exponential ($v \approx 0.6$, "sublocalization") independent of the number of configurations N. In the large ℓ regime, for $\ell \gg \ell_\times(N)$, we find a pronounced dependence on N and a decay faster than exponential ("superlocalization"). This regime is described very well by (30). The crossover point $\ell_\times(N)$ depends logarithmically on N, as suggested by the theoretical description, see (31). The small ℓ regime ($\ell < \lambda_\ell$) is dominated by effects of the wavelength and not it is included into our theoretical description.

Similar results are found for the localization behavior of fractons on percolation clusters on the square lattice and on the simple cubic lattice (Kantelhardt and Bunde 1997). Figure 9 shows our numerical results in ℓ- and r-space on the square lattice. They are very similar to the results for the Cayley tree, as expected. Again the two localization regimes described by (27) and (30) can be observed. In the next section, we will address the localization problem for electronic wave functions which turn out to be very similar to fractons.

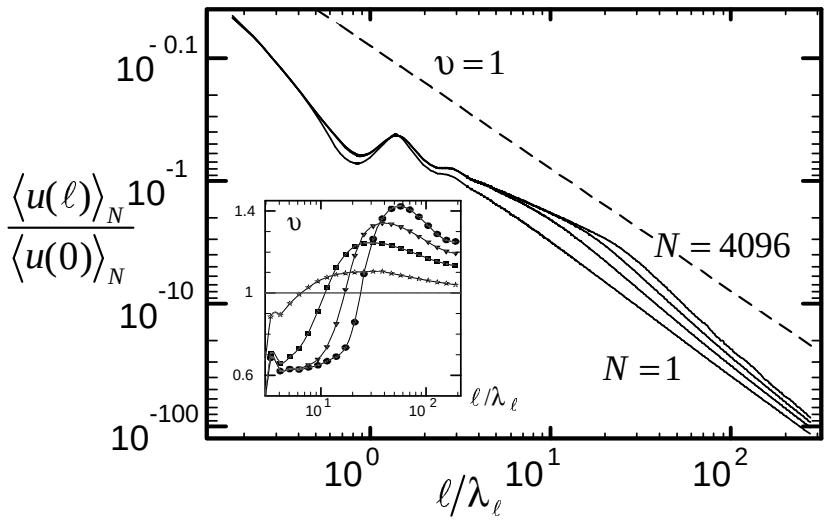

Fig. 8. The decrease of $\langle u(\ell)\rangle_N$ versus ℓ/λ_ℓ for fractons on critical percolation clusters on the Cayley tree for $N = 1$ (bottom line), $N = 8$, $N = 128$, and $N = 4096$ (top line). The value for the localization length, $\lambda_\ell = 5.8$, has been determined from amplitude distributions similar to Fig. 7(a). The straight dashed line has the slope $v = 1$ and is shown for comparison. In the inset, the effective local exponents v determined numerically from the slopes of the curves, are shown versus ℓ/λ_ℓ. The symbols correspond to the effective numbers of configurations: $N = 1$ ($\star$), $N = 8$ (squares), $N = 128$ ($\triangle$), and $N = 4096$ ($\circ$) and the lines are guides to the eye.

5 Electrons

The motion of electrons can be described by hopping between nearest-neighbor cluster sites. Within the tight-binding approximation, the electronic wave function can be written as linear combination of atomic orbitals localized at the cluster sites n. The coefficients $\psi_n(E)$ in the linear combination satisfy the time independent tight-binding equation (Kirkpatrick and Eggarter 1972, Aharony and Harris 1992, Mookerjee et al. 1995)

$$E\ \psi_n(E) = \sum_m{}' V_{n,m}\ \psi_m(E)\,, \tag{32}$$

where again the sum runs over all nearest neighbor sites m of site n. The hopping terms $V_{n,m}$ are constant for nearest neighbor cluster sites and zero otherwise; as above, we will choose $V = 1$ in the following. The "quantum percolation equation" (32) is similar to the scalar vibration equation (24) if the energy eigenvalue E is replaced by $-\omega^2$. The analogy is not complete

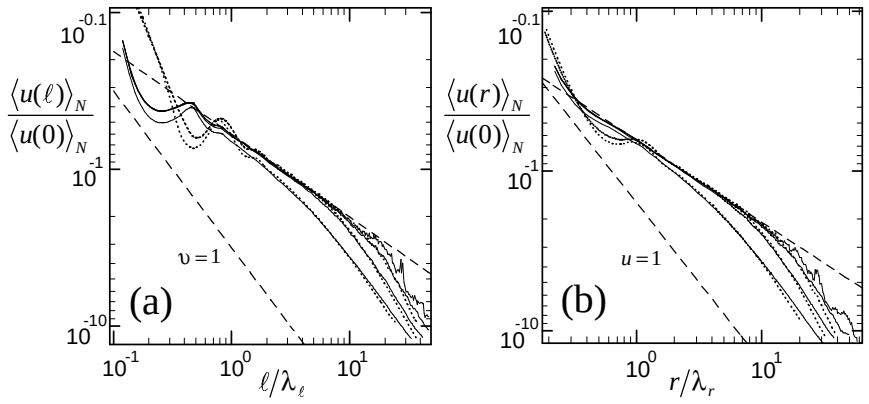

Fig. 9. (a) The decrease of $\langle u(\ell)\rangle_N$ and $\langle \psi(\ell)\rangle_N$ versus ℓ/λ_ℓ for fractons (dotted lines) and electrons (continuous lines) on critical percolation clusters in $d = 2$ for several N-values ($N = 1, 16, 256$ for fractons and $N = 1, 16, 256, 2048$ for electrons; from the bottom to the top). The values for λ_ℓ, $\lambda_\ell = 10.6$ for fractons and $\lambda_\ell = 8.4$ for electrons, have been determined from the corresponding distributions (see Figs. 7(a) and 10(a)). In the intermediate regime, the dashed straight line indicates a fit to the data with an effective localization exponent $\upsilon = 0.53$. (b) The decrease of $\langle u(r)\rangle_N$ and $\langle \psi(r)\rangle_N$ versus r/λ_r for fractons (dotted lines) and electrons (continuous lines) on critical percolation clusters in $d = 2$ for the same eigenfunctions and N-values. The values for λ_r, $\lambda_r = 5.4$ for fractons and $\lambda_r = 4.5$ for electrons, have been determined from the corresponding distributions (see Figs. 7(b) and 10(b)). In the intermediate regime, a dashed straight line indicates a fit to the data with effective localization exponent $u = 0.52$.

though, since the number of nearest neighbor sites N_n does not occur on the left hand side of the tight-binding equation. Thus, the eigenfunctions of (32) and (24) are different.

Despite of these differences, the localization behavior of electrons and fractons turns out to very similar (Kantelhardt and Bunde 1997). This can already be seen in the distributions of the amplitudes $|\psi_n|$ for fixed distances ℓ respectively r from the localization center. Our numerical results for these distributions are shown in Fig. 10 which can be compared to Fig. 7. Since the same log-normal distribution $H(x, \ell)$ of the amplitudes (25) also fits here, the calculation of the averaged amplitudes in the preceeding section is valid for both, electronic wave functions and fractons on critical percolation clusters on the Cayley tree and in $d = 2$ (and $d = 3$). Only the two parameters λ_ℓ and σ have to be adapted. Thus, we obtain the same localization behavior for electrons like for fractons. Our numerical results for the averaged amplitudes of electronic eigenfunctions on percolation clusters at criticality in $d = 2$ are

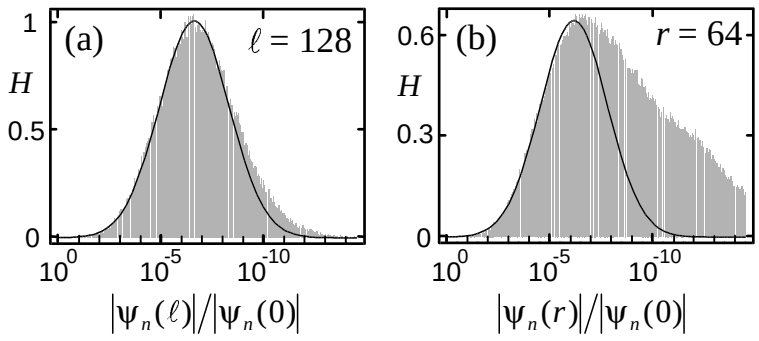

Fig. 10. (a) Histogram of the amplitudes $|\psi_n(\ell)/\psi(0)|$ for electrons on critical percolation clusters in $d = 2$ at fixed chemical lengths $\ell = 128$ from the localization center. (b) Histogram of the amplitude values $|\psi_n(\ell)/\psi(0)|$ for fixed Euclidian lengths $r = 64$. The continuous lines represent Gaussian fits to the data according to (25) and the corresponding function for r-space with the parameters $\lambda_\ell = 8.4$, $\sigma = 2$, $\lambda_r = 4.5$, and $A = 0.65$.

included into Fig. 8, where they can hardly be distinguished from the fracton data.

Acknowledgment

This work was supported by the Deutsche Forschungsgemeinschaft. One of us (J.D.) acknowledges the support of the Hamburger Hochschulsonderprogramm.

References

Aharony, A., Harris, A.B. (1992): Physica A **191**, 365
Alexander, S., Orbach, R. (1982): J. Phys. (Paris) Lett. **43**, L-625
Bouchaud, J.P., Georges, A. (1990): Phys. Rep. **195**, 127
Bunde, A., Havlin, S., Roman, H.E. (1990): Phys. Rev. A **42**, 6274
Bunde, A., Roman, H.E., Russ, St., Aharony, A., Harris, A.B. (1992): Phys. Rev. Lett. **69**, 3189
Bunde, A., Roman, H.E. (1992): Philos. Mag. B **65**, 191
Bunde, A., Dräger, J. (1995): Phys. Rev. E **52**, 53
Bunde, A., Havlin, S., (1996): Eds. *Fractals and Disordered Systems*, 2nd ed. (Springer Verlag, Heidelberg)
Deutscher, G., Levy, Y.-E., Souillard, B. (1987): Europhys. Lett. **4**, 577; Harris, A.B., Aharony, A. (1987): *ibid* **4**, 1355
Dräger, J., Russ, St., Bunde, A. (1995): Europhys. Lett. **31**, 425

Dräger, J., Bunde, A. (1996): Phys. Rev. E **54**, 4596
Eisenberg, E., Havlin, S., Weiss, G.H. (1994): Phys. Rev. Lett. **72**, 2827
Havlin, S., Ben-Avraham, D. (1987): Adv. in Phys. **36**, 695
Klafter, J., Zumofen, G., Blumen, A. (1991): J. Phys. A **24**, 4835
Kantelhardt, J.W., Bunde, A. (1997): Phys. Rev. E **56**, 6693
Kehr, K.W., Kutner, R. (1982): Physica A **110**, 535; Havlin, S. et al. (1985): J. Phys. A **18**, L719
Kirkpatrick, S., Eggarter, T.P. (1972): Phys. Rev. B **6**, 3598
Kramer, B., MacKinnon, A. (1993): Rep. Prog. Phys. **56**, 1469
Lambert, C.J., Hughes, G.D. (1991): Phys. Rev. Lett. **66**, 1074
Levy, Y.-E., Souillard, B. (1987): Europhys. Lett. **4**, 233
Mandal, P., Neumann, A., Jansen, A.G.M., Wyder, P., Deltour, R. (1997): Phys. Rev. B **55**, 452
Montagna, M. et al. (1990): Phys. Rev. Lett. **65**, 1136
Mookerjee, A., Dasgupta, I., Saha, T. (1995): Int. J. Mod. Phys. B **9**, 2989
Nakayama, T., Yakubo, K., Orbach, R.L. (1994): Rev. Mod. Phys. **66**, 381
van der Putten, D., Moonen, J.T., Brom, H.B., Brokken-Zijp, J.C.M., Michels, M.A.J. (1992): Phys. Rev. Lett. **69**, 494; (1993): *ibid* **70**, 4161; Aharony, A., Harris, A.B., Entin-Wohlman, O. (1993): *ibid* **70**, 4160
Sahimi, M. (1994): *Application of Percolation Theory*, Taylor & Francis, London
O'Shaughnessy, B., Procaccia, I. (1985): Phys. Rev. Lett. **54**, 455
Stauffer, D., Aharony, A. (1992): *Introduction to Percolation Theory*, 2nd ed. (Taylor & Francis, London)
Stoll, E., Kolb, M., Courtens, E. (1992): Phys. Rev. Lett. **68**, 2472
Tsujimi, Y. et al. (1988): Phys. Rev. Lett. **60**, 2757
de Vries, P., de Raedt, H., Lagendijk, A. (1989): Phys. Rev. Lett. **62**, 2515; Roman, H.E., Russ, St., Bunde, A. (1991): *ibid* **66**, 1643